Liquid Crystals
Publication details, including instructions for authors and subscription information:
http://www.informaworld.com/smpp/title~content=t713926090

Incommensurability induced by intermolecular hydrogen bonding

Jung-Woo Lee; Jung-Il Jin; M. F. Achard; F. Hardouin

Online publication date: 06 August 2010

To cite this Article Lee, Jung-Woo , Jin, Jung-Il , Achard, M. F. and Hardouin, F.(2001) 'Incommensurability induced by intermolecular hydrogen bonding', Liquid Crystals, 28: 5, 663 — 671
To link to this Article: DOI: 10.1080/02678290010028726
URL: http://dx.doi.org/10.1080/02678290010028726

LIQUID CRYSTALS, 2001, VOL. 28, NO. 5, 663–671

Incommensurability induced by intermolecular hydrogen bonding

JUNG-WOO LEE, JUNG-IL JIN

Center for Electro- and Photo-responsive Molecules and Department of Chemistry, Korea University, Seoul 136-701, Korea

M. F. ACHARD* and F. HARDOUIN

Centre de Recherche Paul Pascal, Université Bordeaux I, Av. A. Schweitzer, 33600 Pessac, France

(*Received 11 September 2000; accepted 22 November 2000*)

Non-symmetric dimesogens are composed of two different mesogenic units linked via a flexible spacer. In this study, a new type of non-symmetric dimesogen has been built through the self-assembly via intermolecular hydrogen bonding between appropriately designed H-bond donor (3-cholesteryloxycarbonylpentanoic acid) and acceptor (aromatic mesogen with a pyridyl group) moieties. As for covalently linked dimesogens, several types of smectic periodicities are observed for these H-bonded cholesteryl compounds depending on the length of the terminal chain of the acceptor moiety: a smectic periodicity resulting from associated dimesogens is observed for long terminal chains, while short chain homologues display an intercalated structure corresponding to half the molecular length. The competition between these two incommensurate lengths can induce an incommensurate smectic phase where the two smectic periodicities coexist at long range.

1. Introduction

It has long been known that in several liquid crystal systems hydrogen bonding is responsible for the existence of the mesophase. The most common example of liquid crystals involving hydrogen bonds between identical molecules concerns benzoic acids [1]. In the last decade Kato and coworkers have exploited H-bonding between two different species to stabilize low molar mass mesophases in binary mixtures [2–5]. Indeed mesogenic structures can be obtained by self-assembly of carboxylic acids as protons donor and pyridyl substituted groups as proton acceptors. The concept of building mesogenic structures through the hydrogen bond between the H-bond donor and acceptor moieties has been extended to a variety of mesogenic compounds [6–16]. Nevertheless, up to now, almost all non-symmetric dimesogens, in which two different mesogenic groups are linked by a flexible spacer, are covalently linked. To our knowledge, only one series of non-symmetric dimesogens has been synthesized through intermolecular hydrogen bonding [11].

The smectic phase behaviour of covalently linked non-symmetric dimesogens appears rather intriguing. Indeed, within the same series, certain homologues form an intercalated smectic phase, in which the layer spacing is close to half the molecular length, while other homologues exhibit smectic phases in which the periodicity is larger than the molecular length [17]. In all the examples, the nature of the smectic phase formed has been found to depend on the relative lengths of the spacer and of the terminal tails [17–19]. Between these two regimes, depending on the series, the smectic phase either vanishes [20] or anomalies of periodicity are revealed through the occurrence of two-dimensional modulated phases [19, 21] and in some rare cases of incommensurate fluid smectic phase S_{ic} [21, 22]. For several years, we have focused on dimesogens composed of a classical aromatic mesogen linked to a cholesteryl moiety by a spacer [18, 22–26]. These compounds denoted as KI-$n(m)$ (where n and m refer to the number of methylene groups in the spacer and the length of the terminal chain, respectively) form smectic phases with a periodicity close to the dimesogen length, labelled as 'S_{q1}' phases, and/or smectic phases with a layer spacing lower than half the molecular length, labelled as 'S_{q3}' phases. The dependence of the smectic layering on the length of the terminal alkyl chain when the spacer length is kept constant shows that the early members exhibit intercalated structures (S_{q3}), while the longer homologues show a 'dimer' modulation (S_{q1}) [24]. A reversed evolution of the layer spacing versus the spacer length is observed: short spacers correspond to a periodicity close to the dimesogen length (S_{q1} phase) and long spacers to S_{q3} phases [18].

*Author for correspondence;
e-mail: achard@crpp.u-bordeaux.fr

Liquid Crystals ISSN 0267-8292 print/ISSN 1366-5855 online © 2001 Taylor & Francis Ltd
http://www.tandf.co.uk/journals
DOI: 10.1080/02678290010028726

However, contrary to other non-symmetric dimesogens, the cholesteryl compounds do not respond to the frustration induced by two incommensurate lengths by destroying the smectic phase, but by inducing smectic phases with anomalies of periodicity. For example, KI-5(4) constitutes an intermediate regime in which the system hesitates between the two periodicities and develops commensurate S_{q1} and S_{q3} phases, incommensurate S_{ic} and two-dimensional fluid smectic phases [21, 22]. In the incommensurate smectic phases evidenced in covalently linked non-symmetric dimesogens [22], the two incommensurate wave vectors $q1$ and $q3$ are collinear and the two competing periodicities coexist at long range.

The objective of the present study was to design similar dimesogenic compounds through H-bonding in order to compare the smectic periodicities of these H-bonded materials with those of the corresponding chemically bonded dimesogens. In particular, the question was to find if anomalies of periodicity can develop with H-bonded compounds or if the latter present only 'classical' smectic arrangements.

The mesogenic 1:1 complexes were prepared from an equimolar mixture of 3-cholesteryloxycarbonylpentanoi c acid (CH6A) as proton donor:

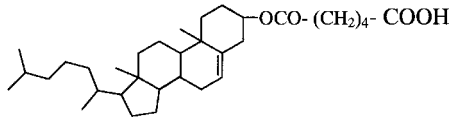

and 4-(pyridin-4-ylmethyleneimino)phenyl 4-alkoxybenzoate (SEOC*n* with $n = 4$ or $n = 10$) as proton acceptor:

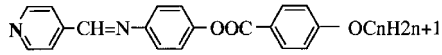

2. Experimental

2.1. *Characterization*

The IR and ^{1}H NMR spectra of all intermediate and final compounds were recorded on a Bomem MB FTIR spectrophotometer and a Bruker AM300 spectrometer, respectively. The thermal behaviour was investigated using a Perkin-Elmer DSC7 differential scanning calorimeter under a nitrogen atmosphere.

The optical textures of the mesophases were observed by polarizing optical microscopy (POM) (Leitz Diavert) in conjunction with a hot stage (FP-82HT) and an automatic controller (Mettler FP-90). When the sample formed a homeotropic texture on a regular glass slide, a rubbed polyimide substrate was used to observe the optical textures.

The mesophase structures were determined by X-ray diffraction (XRD) on powder and aligned samples. For the alignment procedure, the liquid crystal was first introduced by capillarity between two thin glass plates coated with polyimide and unidirectionally rubbed, and then subjected to a mechanical stress perpendicular to the rubbing direction. For the X-ray experiments, the CuK_α radiation from an 18 kW rotating anode X-ray generator (Rigaku-200) was selected by a flat (1 1 1) germanium monochromator. The scattered radiation was collected on a two-dimensional detector (Imaging Plate system from Mar Research, Hamburg). The samples were placed in an oven, providing a temperature control of 0.1 K.

2.2. *Synthesis of CH6A, the compounds SEOCn and the products CH6A-SEOCn*

The synthetic route to the intermediates, CH6A and the compounds, SEOC*n* and to the final pair of materials CH6A-SEOC*n* is shown in the scheme; procedures are summarized below.

2.2.1. *6-Cholesteryloxycarbonylpentanoi c acid, CH6A*

Adipic acid (15.0 g, 0.1 mol) was converted into adipoyl chloride using standard conditions and this was dissolved in 10 ml of a mixture of dry tetrahydrofuran (THF) and pyridine (5:1 by volume). To this solution was added cholesterol (4.0 g, 0.01 mol) dissolved in 10 ml of dry THF. The reaction mixture was stirred for 5 h at room temperature and then 1 h at 60°C under dry nitrogen. The cooled mixture was poured into water and the precipitated product twice purified by recrystallization from diethyl ether and hexane (2:1 by volume). The yield was 4.6 g (87%), m.p. 134°C. FTIR (KBr, cm^{-1}): 3400–2500 (acidic −OH stretching), 2943 (aliphatic C−H stretching), 1722 and 1693 (C=O stretching), 1260 and 1175 (C−O stretching). ^{1}H NMR ($CDCl_3$, ppm): δ 5.4 (m, 1H, −C=CH−), 4.6 (m, 1H, $-(CH_2)_2CH-O-$), 2.4–2.5 (m, 2H, $-CH_2-COOH$), 2.3–2.4 (m, 2H, $-OCO-CH_2-$), 0.6–2.1 (m, 47H, −CH−, $-CH_2-$ and $-CH_3$). Elemental analysis: calc. for $C_{33}H_{54}O_4$ C 76.99, H 10.57; found C 77.00, H 10.61%.

2.2.2. *4-Nitrophenyl 4-butoxybenzoate, **1(4)***

4-Butoxybenzoic (10.1 g, 5.2×10^{-2} mol) was converted into the acid chloride under standard conditions, dissolved in 16 ml of a mixture of dry THF and pyridine (5:1 by volume), and the solution cooled to 0°C. To this solution was added dropwise with vigorous stirring 4-nitrophenol (7.2 g, 5.2×10^{-2} mol) dissolved in 10 ml of dry THF. The temperature was raised to and maintained at 80°C overnight. The reaction mixture was poured into water and the precipitate purified by recrystallization from methanol. The yield was 14.4 g (88%), m.p. 56.5°C. FTIR (KBr, cm^{-1}): 3088 (aromatic C−H stretching), 2958 and 2873 (aliphatic C−H stretching), 1730 (C=O stretching), 1611 and 1512 (aromatic C=C stretching), 1253 and 1159 (C−O stretching). ^{1}H NMR ($CDCl_3$, ppm): δ 8.3 (d, 2H), 8.1 (d, 2H), 7.4 (d, 2H) and 7.0 (d, 2H, aromatic Hs), 4.1 (t, 2H, $-PhOCH_2-$), 1.8 (m, 2H, $-OCH_2CH_2-$), 1.5

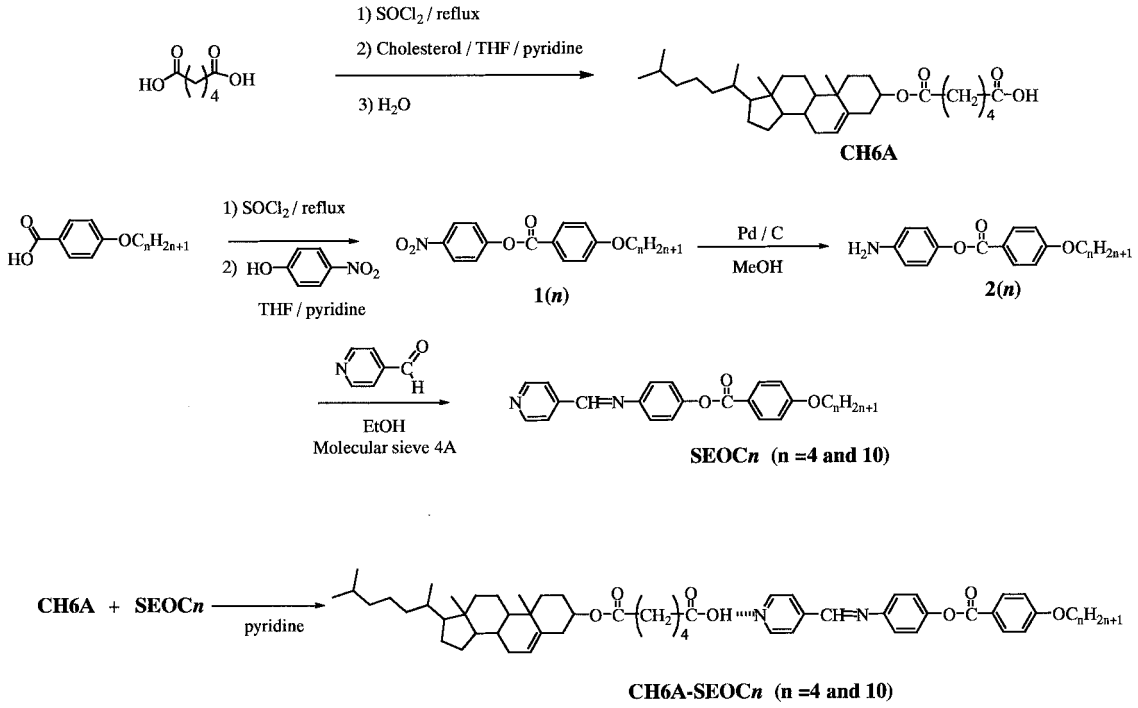

Scheme. Synthetic route to CH6A-SEOC*n*.

(m, 2H, $OCH_2CH_2\underline{CH_2}-$), 1.0 (3H, m, $-\underline{CH_3}$). Elemental analysis: calc. for $C_{17}H_{17}NO_5$ C 64.75, H 5.43, N 4.44; found C 64.80, H 5.51, N 4.42%.

2.2.3. *4-Aminophenyl 4-butoxybenzoate, **2(4)***

Compound **1(4)** (7.5 g, 2.38×10^{-2} mol) was dissolved in 250 ml of methanol. Palladium (10 wt %) with activated charcoal (0.3 g) dispersed in methanol was added and hydrogenation conducted at room temperature for 20 h under normal conditions. The mixture was filtered through celite, the solvent removed, and the product recrystallized from a mixture of methanol and water (4:1 by vol.). The product yield was 5.5 g (81%), m.p. 94°C. FTIR (KBr, cm^{-1}): 3408 and 3298 ($-NH_2$ stretching), 2923 and 2848 (aliphatic C–H stretching), 1722 (C=O stretching), 1608 and 1510 (aromatic C=C stretching), 1255 and 1084 (C–O stretching). ^{1}H NMR ($CDCl_3$, ppm): δ 8.1 (d, 2H), 6.9 (m, 4H) and 6.7 (d, 2H, aromatic Hs), 4.0 (t, 2H, $-PhO\underline{CH_2}-$), 3.5–3.8 (broad, $-\underline{NH_2}$), 1.8 (m, 2H, $-OCH_2\underline{CH_2}-$), 1.5 (m, 2H, $OCH_2CH_2\underline{CH_2}-$), 1.0 (3H, m, $-\underline{CH_3}$). Elemental analysis: calc. for $C_{17}H_{19}NO_3$ C 71.56, H 6.71, N 4.91; found C 71.70, H 6.77, N 4.92%.

2.2.4. *4-(Pyridin-4-ylmethyleneimino)phenyl 4-butoxybenzoate, SEOC4*

Compound **2(4)** (4.0 g, 1.40×10^{-2} mol) and 4-pyridinecarboxaldehyde (1.5 g, 1.4×10^{-2} mol) were dissolved in 25 ml ethanol containing 4 Å molecular sieves. The mixture was then stirred at 80°C for 12 h under a dry nitrogen atmosphere, and insoluble material removed by filtration. After removing the solvent, the crude product was purified by recrystallization from ethanol. The product yield was 2.1 g (40%), m.p. 138.5°C. FTIR (KBr, cm^{-1}): 3064 (aromatic C–H stretching), 2953 (aliphatic C–H stretching), 1720 (C=O stretching), 1605 and 1509 (aromatic C=C stretching), 1260 and 1067 (C–O stretching). ^{1}H NMR ($CDCl_3$, ppm): δ 8.8 (d, 2H), 8.1 (d, 2H), 7.7 (d, 2H) 7.3 (m, 4H) and 7.0 (d, 2H, aromatic Hs), 8.5 (s, $-N=\underline{CH}-$), 4.0 (t, 2H, $-PhO\underline{CH_2}-$), 1.8 (m, 2H, $-OCH_2\underline{CH_2}-$), 1.5 (m, 2H, $OCH_2CH_2\underline{CH_2}-$), 1.0 (3H, m, $-\underline{CH_3}$). Elemental analysis: calc. for $C_{23}H_{22}N_2O_3$ C 73.78, H 5.92, N 7.48; found C 73.70, H 5.99, N 7.45%.

2.2.5. *4-Nitrophenyl 4-decyloxybenzoate, **1(10)***

The product yield was 12.7 g (94%), m.p. 59.5°C. FTIR (KBr, cm^{-1}): 3113 and 3093 (aromatic stretching), 2924 and 2862 (aliphatic C–H stretching), 1734 (C=O stretching), 1613 and 1513 (aromatic C=C stretching), 1259 and 1166 (C–O stretching). ^{1}H NMR ($CDCl_3$, ppm): δ 8.3 (d, 2H), 8.1 (d, 2H), 7.4 (d, 2H) and 7.0 (d, 2H, aromatic Hs), 4.1 (t, 2H, $-PhO\underline{CH_2}-$), 1.8 (m, 2H, $-OCH_2\underline{CH_2}-$), 1.3–1.6 (m, 14H, $\underline{OCH_2CH_2(CH_2)_7}-$), 0.9 (3H, m, $-\underline{CH_3}$). Elemental analysis: calc. for $C_{23}H_{29}NO_5$ C 69.15, H 7.32, N 3.51; found C 69.24, H 7.42, N 3.49%.

2.2.6. *4-Aminophenyl 4-decyloxybenzoate, **2(10)***

The product yield was 4.5 g (62%), m.p. 96°C. FTIR (KBr, cm^{-1}): 3463 and 3369 ($-NH_2$ stretching), 2923 and 2848 (aliphatic C–H stretching), 1722 (C=O stretching), 1608 and 1510 (aromatic C=C stretching), 1255 and 1084 (C–O stretching). ^1H NMR ($CDCl_3$, ppm): δ 8.1 (d, 2H), 7.0 (m, 4H) and 6.7 (d, 2H aromatic Hs), 4.0 (t, 2H, $-PhOCH_2-$), 3.7 ~ 3.8 (broad, $-NH_2$), 1.8 (m, 2H, $-OCH_2CH_2-$), 1.3 ~ 1.6 (m, 14H, $OCH_2CH_2(CH_2)_7-$), 0.9 (3H, m, $-CH_3$). Elemental analysis: calc. for $C_{23}H_{31}NO_3$ C 74.76, H 8.46, N 3.79; found C 74.75, H 8.50, N 3.78%.

2.2.7. *4-(Pyridin-4-ylmethyleneimino)phenyl 4-decyloxybenzoate, SEOC10*

The product yield was 2.5 g (42%), m.p. 94°C. FTIR (KBr, cm^{-1}): 3053 (aromatic C–H stretching), 2917 and 2829 (aliphatic C–H stretching), 1718 (C=O stretching), 1605 and 1509 (aromatic C=C stretching), 1257 and 1075 (C–O stretching). ^1H NMR ($CDCl_3$, ppm): δ 8.7 (d, 2H), 8.1 (d, 2H) 7.7 (d, 2H), 7.2 (m, 4H) and 7.0 (d, 2H aromatic Hs), 8.5 (s, $-N=CH-$), 4.0 (t, 2H, $-PhOCH_2-$), 1.8 (m, 2H, $-OCH_2CH_2-$), 1.3–1.6 (m, 14H, $OCH_2CH_2(CH_2)_7-$), 0.9 (3H, m, $-CH_3$). Elemental analysis: calc. for $C_{29}H_{34}N_2O_3$ C 75.95, H 7.47, N 6.11; found C 75.98, H 7.53, N 6.12%.

2.3. *Preparation of hydrogen-bonded complexes*

Both complexes dealt with in this study were prepared similarly and the method for the hydrogen-bonded complex CH6A-SEOC4 is described as an example.

2.3.1. *CH6A-SEOC4*

CH6A (0.340 g, 6.60×10^{-4} mol) and SEOC4 (0.247 g, 6.60×10^{-4} mol) were dissolved in 5 ml of pyridine. The mixture was heated at 40°C and then the pyridine was removed under reduced pressure. The resulting solid complex was dried under vacuum at 60°C for 12 h. FTIR (KBr, cm^{-1}): 2941 and 2868 (aliphatic C–H stretching), 2652–2236 and 2051–1790 (hydrogen bond O–H stretching), 1730 (C=O stretching), 1606 and 1509 (aromatic C=C stretching), 1255 and 1069 (C–O stretching). ^1H NMR ($CDCl_3$, ppm): δ 8.8 (d, 2H), 8.1 (d, 2H) 7.8 (d, 2H), 7.3 (m, 4H) and 7.0 (d, 2H aromatic Hs), 8.5 (s, $-N=CH-$), 5.4 (m, 1H, $-C=CH-$), 4.6 (m, 1H, $-(CH_2)_2CH-O-$), 4.0 (t, 2H, $-PhOCH_2-$), 2.4–2.5 (m, 2H, $-CH_2-COOH$), 0.6–2.1 (m, 54H, $-CH-$, $-CH_2-$ and $-CH_3$). Elemental analysis: calc. for $C_{56}H_{76}N_2O_7$ C 75.67, H 8.62, N 3.17; found C 75.67, H 8.62, N 3.17%.

2.3.2. *CH6A-SEOC10*

FTIR (KBr, cm^{-1}): 3053 (aromatic C–H stretching), 2934 and 2863 (aliphatic C–H stretching), 2750–2300 and 2060–1800 (hydrogen bond O–H stretching), 1734 (C=O stretching), 1607 and 1509 (aromatic C=C stretching), 1256 and 1067 (C–O stretching). ^1H NMR ($CDCl_3$, ppm): δ 8.8 (d, 2H), 8.1 (d, 2H) 7.8 (d, 2H), 7.3 (m, 4H) and 7.0 (d, 2H aromatic Hs), 8.5 (s, $-N=CH-$), 5.4 (m, 1H, $-C=CH-$), 4.6 (m, 1H, $-(CH_2)_2CH-O-$), 4.0 (t, 2H, $-PhOCH_2-$), 2.4–2.5 (m, 2H, $-CH_2-COOH$), 0.6–2.1 (m, 66H, $-CH-$, $-CH_2-$ and $-CH_3$). Elemental analysis: calc. for $C_{62}H_{88}N_2O_7$ C 76.50, H 9.11, N 2.88; found C 76.53, H 9.22, N 2.87%.

3. Results and discussion

The thermal transitions of the H-bonding donor and acceptor moieties (CH6A and SEOC4 and SEOC10) and of the 1:1 complexes (CH6A-SEOC4 and CH6A-SEOC10) were examined by DSC, following initial characterization of the liquid crystalline phases by POM XRD experiments were performed to obtain structural identification. Results are summarized in the table.

3.1. *Mesomorphic properties*

The compound CH6A shows an enantiotropic cholesteric phase with classical oily streaks or fan-shaped textures. SEOC4 is purely nematic, while for the compound SEOC10, a nematic–smectic A–smectic C phase sequence is observed. The 1:1 complexes CH6A-SEOC4 and CH6A-SEOC10 behave as single component liquid crystalline materials and exhibit stable mesophases.

Table. Transition temperatures (by POM) and enthalpies for the H-bonding donor and acceptor precursors and for the 1:1 H-bonded complexes.

Compound	Transition temperature (°C) and enthalpy [kJ mol^{-1}]
CH6A	Cr [24.5] 134 N* [1.5] 148 I
SEOC4	Cr [40.9] 138.5 N [0.4] 160 I
SEOC10	Cr [40.9] 94 SmC [–][a] 133 SmA [1.6] 143 N [0.8] 145 I
CH6A-SEOC4	Cr [40.8] 126 SmHT[b] [0.18] 145 N* [3.95] 192 I (SmLT 116)[c] [0.18]
CH6A-SEOC10	Cr [38.7] 126 Sm [0.25] 135 N* [5.6] 192 I

[a] Very small enthalpy value.
[b] High temperature smectic.
[c] Low temperature smectic.

The DSC data in figures 1(*b*) and 2(*b*) confirm that the isotropization temperatures increase noticeably for the 1:1 complexes by comparison with the precursors: the mesomorphic range of the mixtures was extended to 66 and 70°C as compared with 14°C for CH6A and 21.5 and 51°C for SEOC4 and SEOC10, respectively. The strong stabilization of the mesophases is due to the formation of 'H-bonded non-symmetric dimesogens'.

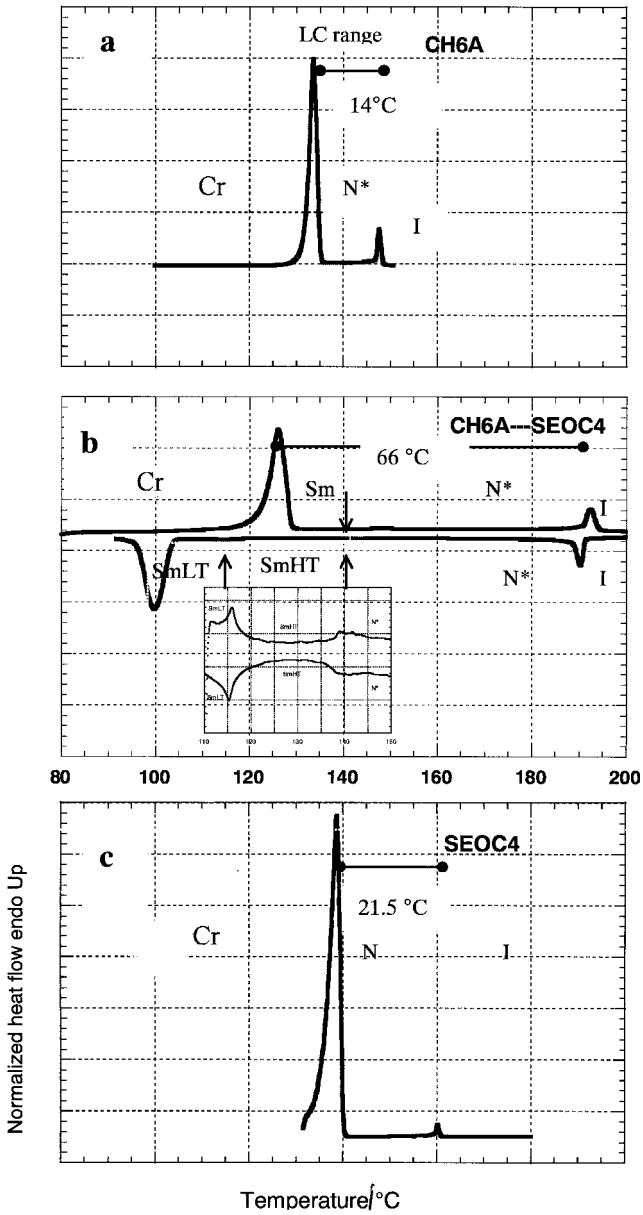

Figure 1. DSC thermograms of (*a*) CH6A, (*b*) CH6A-SEOC4 complex, (*c*) SEOC4 on heating (5°C min^{-1}): (*b*) shows the thermograms on heating and cooling for the complex and the insert shows the reversibility of the transition between the two smectic phases in a supercooled temperature range.

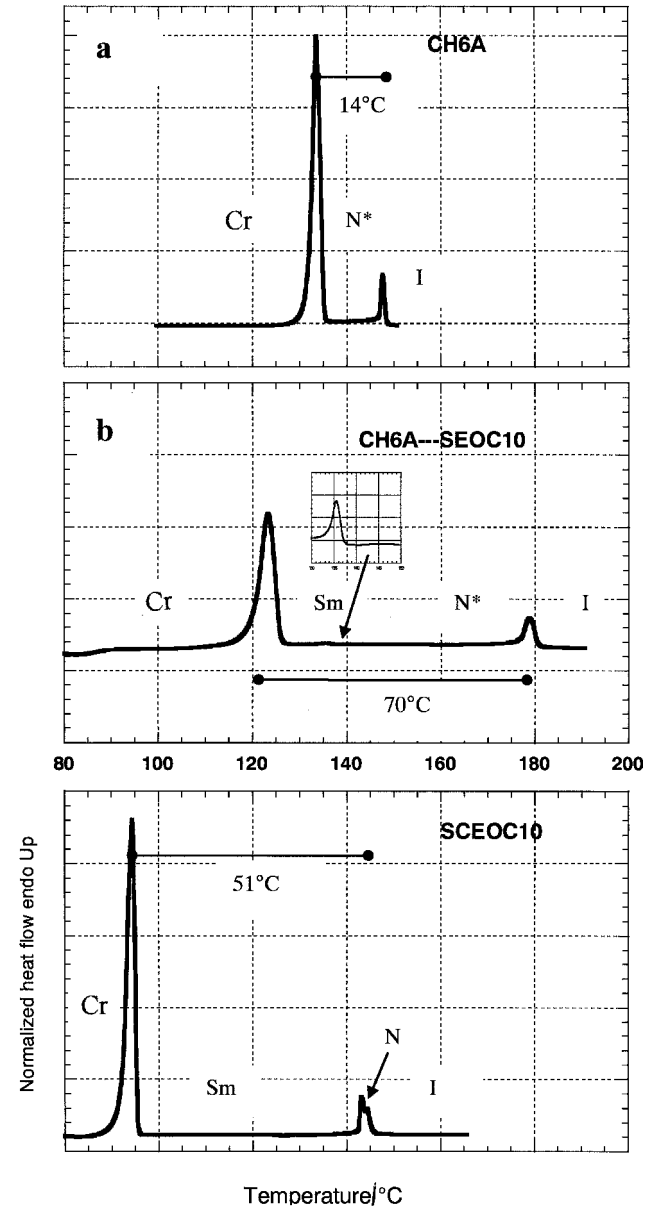

Figure 2. DSC thermograms of (*a*) CH6A, (*b*) CH6A-SEOC10 complex, (*c*) SEOC10 on heating (5°C min^{-1}).

The existence of intermolecular hydrogen bonds in the 1:1 CH6A-SEOC*n* complexes can be confirmed by FTIR spectroscopy. Infrared spectra of CH6A and CH6A-SEOC4 in the range 1500–3400 cm^{-1} are shown in figure 3. From the spectra of CH6A the broad band of the OH group of the carboxyl group centred at 3000 cm^{-1} and bands around 2560 and 2670 cm^{-1}, and two carbonyl bands at 1732 cm^{-1} (ester carbonyl) and 1705 cm^{-1} (carboxylic) are seen. The O–H bands at 2475 and 1910 cm^{-1} observed in the IR spectra of the CH6A-SEOC4 complex are indicative of strong hydrogen bonding between the carboxyl and pyridyl

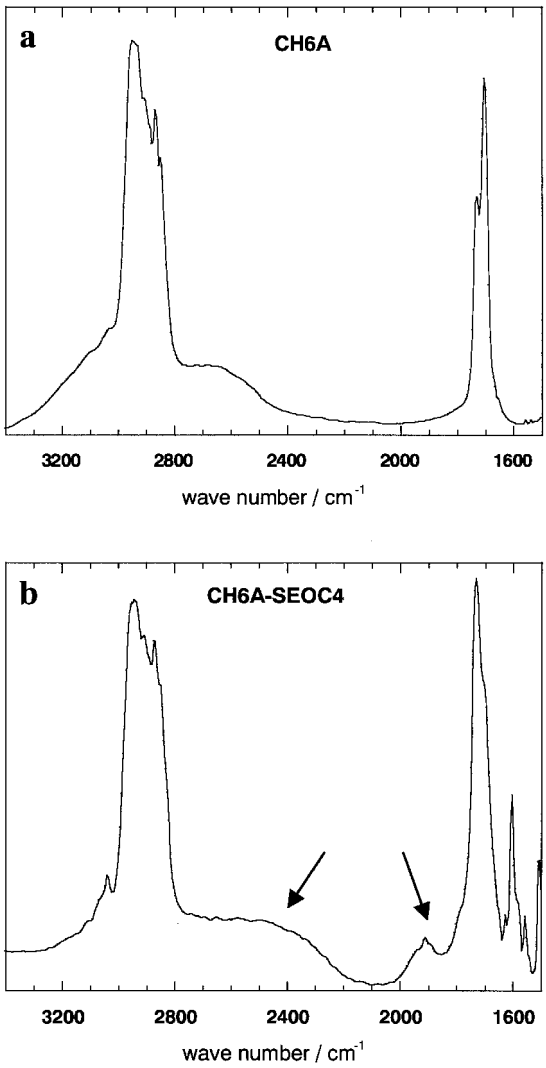

Figure 3. Infrared spectra of CH6A (*a*) and CH6A-SEOC4 (*b*) in the range 1500–3400 cm^{-1} at room temperature.

units [3, 27, 28]. At the same time, the ester carbonyl bands of SEOC4 and of CH6A merge into one and the carboxylic carbonyl band shifts to 1689 cm^{-1} due to the intermolecular hydrogen bonding.

As already observed in several systems, mesophases are often induced through intermolecular hydrogen bonding. In the present case, a smectic domain is induced for the CH6A-SEOC4 complex, since neither CH6A nor SEOC4 exhibits a smectic phase, and this observation constitutes another probe of the formation of a new dimesogenic unit obtained through intermolecular hydrogen bonding.

As noted in the table, the 1 : 1 CH6A-SEOC4 complex displays two smectic phases. With untreated glass plates, the cholesteric phase is characterized by a focal-conic texture and the onset of the smectic phase is revealed by the complete extinction of the homeotropic alignment. By using rubbed polyimide glass, a focal-conic texture with narrow ellipses is observed for the high temperature (HT) smectic phase, figure 4 (*a*). The monotropic SmHT–SmLT transition is only revealed by a multiplication of the number of focal-conic groups, figure 4 (*b*).

The precursor SEOC10 forms a cholesteric–smectic A–smectic C phase sequence. However, the complex CH6A-SEOC10 exhibits only a cholesteric and a smectic C phase (figure 5).

XRD studies were performed on the precursor SEOC10 and the two CH6A-SEOC*n* complexes in the different smectic phases.

3.2. *Structural properties*

The smectic phases of SEOC10, CH6A-SEOC10 and CH6A-SEOC4 exhibit Bragg peaks in the low angle region corresponding to the layer reflections, and diffuse scattering at wide angle which gives evidence of a liquid-like order within the layers.

For the SEOC10 precursor, the layer spacing d is constant in the smectic A phase, and decreases from 35.1 to 33.8 Å with decreasing temperature in the smectic C phase, indicating the increase in tilt angle (which reaches 15° at 100°C). The smectic A phase is partially bilayer, since the layer spacing (35.1 Å) is larger than the molecular length in the most extended conformation (30.5 Å).

The smectic phase of the CH6A-SEOC10 complex is a chiral smectic C phase and the layer spacing decreases from 52 Å ($q = 0.120$ $Å^{-1}$) to 45 Å ($q = 0.139$ $Å^{-1}$) with decreasing temperature. It is worth noting that in the smectic phase of the complex, the layer parameter is considerably larger than in the case of the SEOC10 precursor (as illustrated in figure 6).This result confirms the selective formation of the hydrogen-bonded dimesogen between the acid derivative and the pyridyl mesogen. A comparison of the d-spacing with the length of this new extended dimesogen (57 Å in the most extended conformation) suggests a rather large tilt angle.

The high temperature smectic phase of the CH6A-SEOC4 complex is probably a smectic A phase (see textures). As shown in figure 7, in this phase the intensity profile in the low angle region displays a Bragg peak at $q = 0.266$ $Å^{-1}$ (23.6 Å) and an additional diffuse scattering centred around $q = 0.104$ $Å^{-1}$ (60.4 Å). This diffuse scattering becomes more visible as the temperature decreases in this high temperature smectic phase.

The signature of the low temperature smectic phase of the CH6A-SEOC4 complex (115°C) is the condensation of this diffuse scattering into a Bragg reflection and SmLT exhibits two incommensurate peaks at $q = 0.104$ $Å^{-1}$ (60.4 Å) and $q = 0.266$ $Å^{-1}$ (23.6 Å). The corresponding oriented pattern shown in figure 8 undoubtedly reveals that the two incommensurate wave vectors are collinear

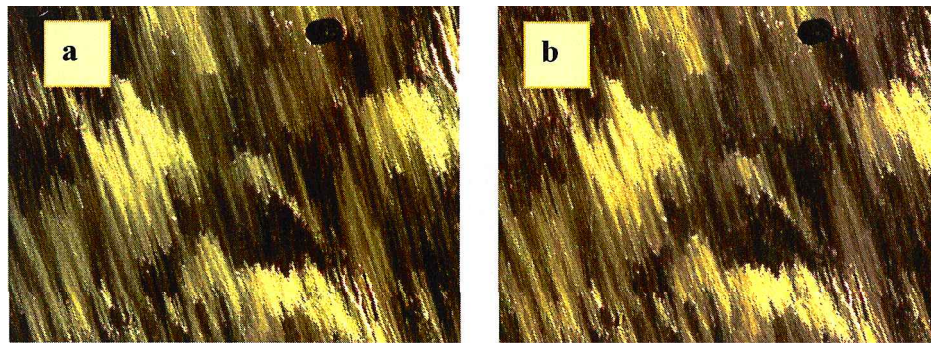

Figure 4. 1:1 CH6A-SEOC4 complex: (*a*) high temperature smectic SmHT (136°C), (*b*) low temperature smectic SmLT (113°C).

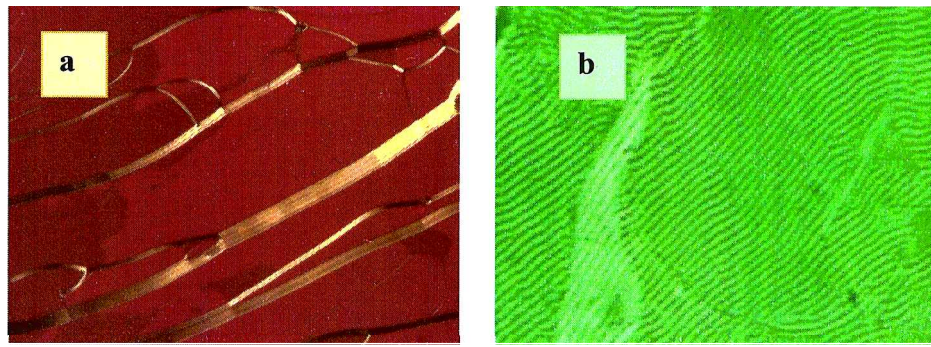

Figure 5. CH6A-SEOC10 complex on a rubbed polyimide surface: (*a*) cholesteric texture with oily streaks at 144°C; (*b*) texture at 126°C of chiral smectic C when the plane layers dip at an angle to the glass surface. The equally spaced lines are related to the pitch of the phase.

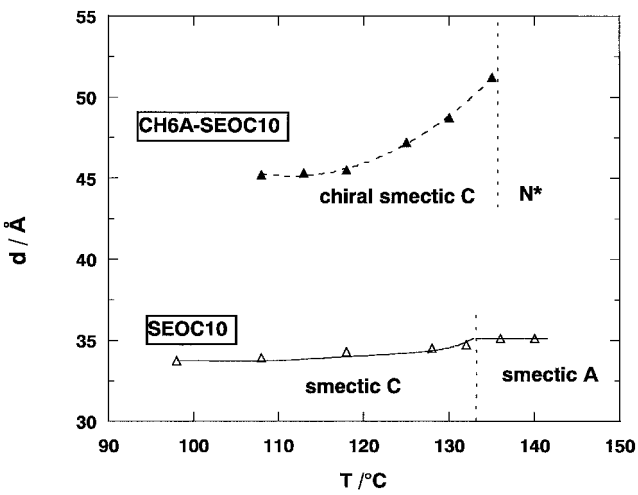

Figure 6. Thermal evolution of the layer spacing for the SEOC10 precursor (open symbols) and for the CH6A-SEOC10 complex (filled symbols).

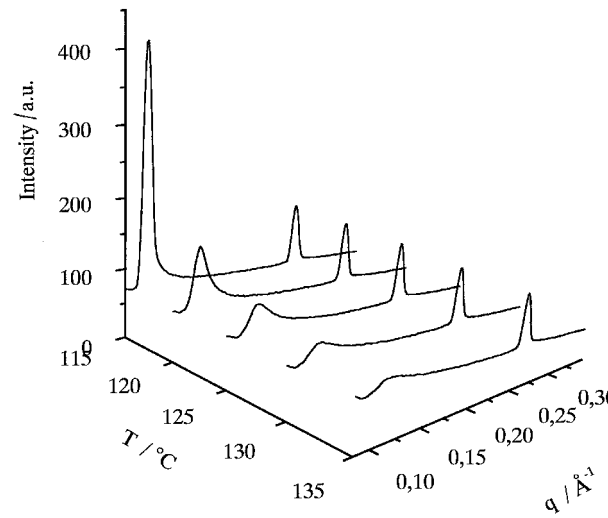

Figure 7. Thermal evolution of the intensity profiles in the low angle region for the CH6A-SEOC4 complex: the high temperature smectic phase displays a Bragg peak at $q = 0.266$ Å^{-1}. An additional diffuse scattering centred around $q = 0.104$ Å^{-1} becomes more and more visible as the temperature decreases in the high temperature smectic phase. The occurrence of the low temperature smectic phase (115°C) is characterized by the condensation of this diffuse scattering into a Bragg reflection: SmLT exhibits two incommensurate peaks at $q = 0.104$ Å^{-1} (60.4 Å) and $q = 0.266$ Å^{-1} (23.6 Å).

and this is the sign of the occurrence of an incommensurate fluid smectic S_{ic} (probably smectic A) in this H-bonded dimesogen.

As in our previous papers on covalently linked dimesogens [18, 21, 26], we can use here a nomenclature based on the smectic periodicity rather than on the smectic C

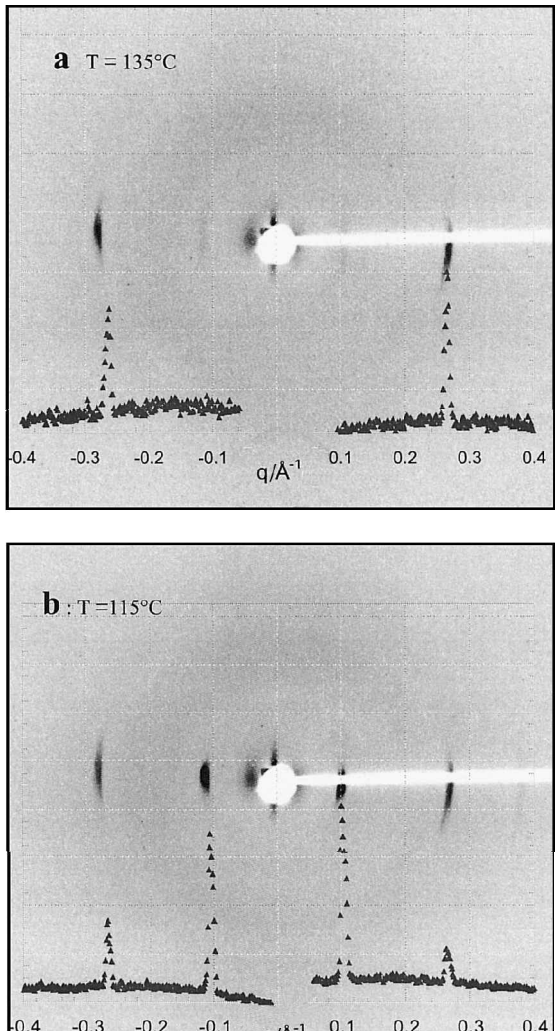

Figure 8. Oriented X-ray patterns for the CH6A-SEOC4 complex: (*a*) in the high temperature smectic phase (135°C), a Bragg reflection at $q = 0.266$ Å^{-1} and a weak diffuse scattering centred at $q = 0.104$ Å^{-1} are seen; (*b*) in the low temperature smectic phase (115°C) two collinear Bragg reflections corresponding to the incommensurate wave vectors $q = 0.104$ Å^{-1} (60.4 Å) and $q = 0.266$ Å^{-1} (23.6 Å) are clearly detected suggesting an incommensurate fluid smectic phase.

or smectic A nature of the phase: when the periodicity is larger than (or close to) the dimesogen length, the smectic phase is labelled the 'S_{q1} phase' ($q1$ is the wave vector) and when the layer spacing is lower than (or close to) half the molecular length, the phase is called the 'S_{q3} phase' ($q3$ is the wave vector). In summary, the CH6A-SEOC10 complex exhibits an S_{q1} phase and the CH6A-SEOC4 complex an S_{q3} phase. Thus we observe the same inversion of the smectic periodicity versus the terminal chain length as in covalently linked dimesogens [24]: S_{q1} for long tails and S_{q3} for short tails. In addition, the competition between these two incommensurate periodicities is revealed in the CH6A-SEOC4 complex as previously observed for the KI-5(4) covalently linked dimesogen. The results presented here demonstrate that the H-bonded dimesogens behave as single components with properties comparable to those of covalently linked dimesogens.

Finally, mixtures can be prepared with any ratio of the proton donor and acceptor and the use of non-stochiometric mixtures provides another degree of freedom for fine-tuning the mesomorphic and structural properties.

References

[1] See for example: Bradfield, A. E., and Jones, B., 1929, *J. chem. Soc.*, 2660; Gray, G. W., and Jones, B., 1953, *J. chem. Soc.*, 4179.
[2] Kato, T., and Frechet, J. M. J., 1989, *J. Am. chem. Soc.*, **111,** 8533.
[3] Kato, T., Uryu, T., Kaneuchi, F., Jin, C., and Frechet, J. M. J., 1993, *Liq. Cryst.*, **14,** 1311.
[4] Kato, T., Kihara, H., Uryu, T., Ujiie, S., Iimura, K., Frechet, J. M. J., and Kumar, U., 1993, *Ferroelectrics*, **148,** 161.
[5] Kato, T., Fuku Masa, M., and Frechet, J. M. J., 1995, *Chem. Mater.*, **7,** 368.
[6] Kato, T., and Frechet, J. M. J., 1989, *Macromol.*, **22,** 3818.
[7] Kumar, U, Kato, T., and Frechet, J. M. J., 1992, *J. Am. chem. Soc.*, **114,** 6630.
[8] Yu, L. J., 1993, *Liq. Cryst.*, **14,** 1303.
[9] Wilson, L. M., 1994, *Macromolecules*, **27,** 6683.
[10] Kato, T., Hirota, N., Fujishima, A., and Frechet, J. M. J., 1996, *J. polym. Sci., polym. Chem.*, **34,** 57.
[11] Tian, Y., Xu, X., Zhao, Y., Tang, X., and Li, T., 1997, *Liq. Cryst.*, **22,** 87.
[12] Kumar, P. A., Srinivasulu, M., and Pisipati, G. K. M., 1999, *Liq. Cryst.*, **26,** 1339.
[13] Hu, H., Kang, N., Xi, P., Zhang, R.-B., and Xu, D.-F., 2000, *Liq. Cryst.*, **27,** 169.
[14] Gündogan, B., and Binnemans, K., 2000, *Liq. Cryst.*, **27,** 851.
[15] Ihata, O., Yokota, H., Kanie, K., Ujiie, S., and Kato, T., 2000, *Liq. Cryst.*, **27,** 69.
[16] Lin, H.-C., Shiaw, J.-M., Wu, C-Y., and Tsai, C., 2000, *Liq. Cryst.*, **27,** 1103.
[17] Attard, G. S., Date, R. W., Imrie, C. T., Luckhurst, G. R., Roskilly, S., Seddon, J. M., and Taylor, L., 1994, *Liq. Cryst.*, **16,** 529.
[18] Hardouin, F., Achard, M. F., Jin, J.-I., and Yun, Y.-K., 1995 *J. Phys. II Fr.*, **5,** 927.
[19] Faye, V., Nguyen, H. T., and Barois, P., 1997, *J. Phys. II Fr.*, **7,** 1245.
[20] Hogan, J. L., Imrie, C. T., and Luckhurst, G. R., 1988, *Liq. Cryst.*, **3,** 645.
[21] Hardouin, F., Achard, M. F., Jin, J.-I., Yun, Y.-K., and Chung, S. J., 1998, *Eur. Phys. J. B*, **1,** 47.
[22] Hardouin, F., Achard, M. F., Jin, J.-I., Shin, J.-W., and Yun, Y.-K., 1994, *J. Phys. II Fr.*, **4,** 627.

[23] Jin, J.-I., 1995 *Mol. Cryst. liq. Cryst.*, **267,** 249.
[24] Hardouin, F., Achard, M. F., Laguerre, M., Jin, J.-I., and Ko, D.-H., 1999, *Liq. Cryst.*, **26,** 589.
[25] Cha, S. W., Jin, J.-I., Laguerre, M., Achard, M. F., and Hardouin, F., 1999, *Liq. Cryst.*, **26,** 1325.
[26] Lee, D. W., Jin, J.-I., Laguerre, M., Achard, M. F., and Hardouin, F., 2000, *Liq. Cryst.*, **27,** 145.
[27] Johnson, S. L., and Rumon, K. A., 1965, *J. phys. Chem.*, **69,** 74.
[28] Odinokov, S. E., and Iogansen, A. V., 1972, *Spectrochim. Acta A*, **28,** 2343.